


**Magnetism and superconductivity in mixed-dimensional periodic Anderson model for  $\text{UTe}_2$** Ryuji Hakuno,\* Kosuke Nogaki , and Youichi Yanase*Department of Physics, Graduate School of Science, Kyoto University, Kyoto 606-8502, Japan*

(Received 31 May 2023; revised 28 December 2023; accepted 6 February 2024; published 18 March 2024)

$\text{UTe}_2$  is a strong candidate for a topological spin-triplet superconductor, and it is considered that the interplay of magnetic fluctuation and superconductivity is essential for the origin of the superconductivity. Despite various experiments suggesting ferromagnetic criticality, neutron scattering measurements observed only antiferromagnetic fluctuation and called for theories of spin-triplet superconductivity near the antiferromagnetic quantum critical point. We construct a periodic Anderson model with one-dimensional conduction electrons and two- or three-dimensional  $f$  electrons, reminiscent of the band structure of  $\text{UTe}_2$ , and show that ferromagnetic and antiferromagnetic fluctuations are reproduced depending on the Fermi surface of  $f$  electrons. These magnetic fluctuations cooperatively stabilize spin-triplet  $p$ -wave superconductivity. We also study hybridization dependence as a possible origin of the pressure-induced superconducting phase transition and find that moderately large hybridization changes the antiferromagnetic wave vector and stabilizes  $d$ -wave superconductivity.

DOI: [10.1103/PhysRevB.109.104509](https://doi.org/10.1103/PhysRevB.109.104509)**I. INTRODUCTION**

Spin-triplet superconductivity is an exotic quantum condensed state of matter. Interest in spin-triplet superconductors is growing as they are platforms of multicomponent superconductivity, bulk topological superconductivity [1–4], and superconducting spintronics [5]. Since the discovery of superconductivity [6],  $\text{UTe}_2$  has been considered to be a spin-triplet superconductor candidate, and intensive studies have been devoted to clarifying the superconducting states in  $\text{UTe}_2$  [7]. One of the authors previously predicted the topological superconductivity in  $\text{UTe}_2$  [8]. However, the topological indices and the presence/absence of Majorana fermions depend on the symmetry of the superconducting gap function and the topology of Fermi surfaces. Therefore, a thorough study of the electronic structure, pairing mechanism, and superconducting states is desirable.

In early studies, the ferromagnetic quantum critical fluctuation has been indicated [6,9,10] and considered to be a glue of spin-triplet Cooper pairs. However, the neutron scattering experiments detected an antiferromagnetic fluctuation [11–14] with the wave vector around  $\mathbf{q} \simeq (0, \pi, 0)$  and called for a search for spin-triplet superconductivity arising from the antiferromagnetic fluctuation. Although the spin-triplet pairing interaction can be mediated by antiferromagnetic fluctuations [15,16], spin-singlet superconductivity was shown to be more stable in most cases [15,17,18]. Magnetic anisotropy and its coupling to electrons have been assumed phenomenologically to show stable spin-triplet superconductivity [19–22]. However, an analysis of the multiorbital Hubbard model with spin-orbit coupling has not supported the assumption [23]. Although charge fluctuation has also been investigated for possible spin-triplet superconductivity in organic systems [15,18,24,25], its applicability to

heavy-fermion superconductors remains to be verified. Therefore, the construction of a microscopic model for spin-triplet superconductivity and antiferromagnetic fluctuation is essential for the research of  $\text{UTe}_2$ .

To study the relationship between magnetic fluctuations and superconductivity, information on the electron band structure is indispensable [16]. An angle-resolved photoemission spectroscopy (ARPES) experiment [26] observed quasi-two-dimensional Fermi surfaces consistent with the density functional theory plus  $U$  (DFT+ $U$ ) [8] and DFT plus dynamical mean-field theory (DFT+DMFT) calculations [26,27] for a large Coulomb interaction. Indication of a three-dimensional Fermi surface was also reported [26], but it is under debate [28]. Recent developments in crystal growth [29] enabled quantum oscillation measurements [30–33], which precisely detected quasi-two-dimensional Fermi surfaces in the high magnetic field region. However, rather three-dimensional bulk properties such as superconducting coherence length [34] and electrical conductivity [35] have been observed, and the presence or absence of a three-dimensional Fermi surface is still controversial and requires further study at zero or low magnetic fields.

Inspired by the experimental studies of magnetic fluctuations and band structure in  $\text{UTe}_2$ , we study a microscopic model with the Fermi surfaces consistent with the band-structure calculations [8,26,27,36] and show spin-triplet superconductivity near the antiferromagnetic quantum critical point. Although several theoretical models were proposed for  $\text{UTe}_2$  [16,36–42], a microscopic model reproducing antiferromagnetic fluctuation, Fermi surfaces, and spin-triplet superconductivity was not reported. In this paper, we propose a mixed-dimensional periodic Anderson model (PAM) and reveal antiferromagnetic fluctuation and spin-triplet superconductivity coherently.

Typical uranium-based heavy-fermion superconductors, such as  $\text{UCoGe}$  and  $\text{URhGe}$ , exhibit changes in the nature of superconductivity when subjected to pressure and magnetic

\*hakuno.ryuji.46v@st.kyoto-u.ac.jp

fields [43]. More interestingly, the application of pressure or magnetic fields to  $\text{UTe}_2$  revealed multiple superconducting phases [44–55], suggesting that the external fields change the electronic state and superconductivity. Thus, we also investigate the variation of superconducting states associated with the change of the Fermi surfaces in our PAM.

## II. MODEL AND METHOD

With a tight-binding model for  $f$ ,  $d$ , and  $p$  electrons as a noninteracting part  $H_0$ , the mixed-dimensional PAM is given by  $H = H_0 + H_1$ , where

$$H_0 = H_f + H_d + H_p + H_{fd} + H_{fp} + H_{dp}, \quad (1)$$

$$H_m = \sum_{k\sigma} [\varepsilon_m(\mathbf{k}) - \mu] a_{mk\sigma}^\dagger a_{mk\sigma} \quad (m = f, d, p), \quad (2)$$

$$H_{ml} = \sum_{k\sigma} V_{ml} a_{mk\sigma}^\dagger a_{lk\sigma} + \text{H.c.} \quad (ml = fd, fp, dp), \quad (3)$$

and  $H_1 = U \sum_j n_{fj\uparrow} n_{fj\downarrow}$  is the on-site Coulomb interaction of  $f$  electrons. The mixed-dimensional property of the model is represented in the kinetic energies,

$$\varepsilon_f(\mathbf{k}) = -2t_{fx} \cos k_x - 2t_{fy} \cos k_y + 2t_{fz}(\cos k_z + 1) + \Delta_f, \quad (4)$$

$$\varepsilon_d(\mathbf{k}) = -2t_{dx} \cos k_x - 2t_{dy} \cos k_y + \Delta_d, \quad (5)$$

$$\varepsilon_p(\mathbf{k}) = 2t_{px} \cos k_x + 2t_{py} \cos k_y + \Delta_p. \quad (6)$$

Here, we assume quasi-one-dimensional conduction electrons in accordance with the band structure of  $\text{UTe}_2$  [8,26,27,37]. In  $\text{UTe}_2$ , the  $d$  and  $p$  electrons mainly conduct along the  $a$  and  $b$  axis, respectively, corresponding to  $t_{dx} \gg t_{dy}$  and  $t_{px} \ll t_{py}$ . We also assume three-dimensional  $f$  electrons with comparable hopping integrals  $t_{fx}$ ,  $t_{fy}$ , and  $t_{fz}$ . Thus, conduction electrons and  $f$  electrons have nonequivalent dimensionality, and we call the Hamiltonian the (1 + 3)-dimensional PAM. The (1 + 2)-dimensional PAM can also be constructed by simply setting  $t_{fz} = 0$ . The results of the (1 + 2)-dimensional model are shown in the Supplemental Material for comparison [56].

The crystal fields are denoted by  $\Delta_{p,d,f}$ , and we adopt momentum-independent hybridization terms for simplicity. Later, we show that the  $f$ -electron level  $\Delta_f$  and the hybridization with  $p$  electrons  $V_{fp}$  are the control parameters of the model. We set  $V_{fp} = 0.05$  unless mentioned otherwise. In the following discussions, we fix the other parameters ( $t_{fx}, t_{fy}, t_{fz}, t_{dx}, t_{dy}, \Delta_d, t_{px}, t_{py}, \Delta_p, V_{fd}, V_{dp}, \mu$ ) = (0.08, 0.035, 0.1, 0.5, 0, 0, 0, 1, 0, 0.05, 0.05, -0.1) and the temperature  $T = 0.01$ .

The noninteracting Green's function is defined as  $\hat{G}(k) = (i\omega_n \hat{I} - \hat{H}_0)^{-1}$ , where  $k = (\mathbf{k}, i\omega_n)$ ,  $\omega_n = (2n + 1)\pi T$  are fermionic Matsubara frequencies, and  $\hat{I}$  is the identity matrix. The spin and charge susceptibilities are evaluated by the random phase approximation (RPA) as

$$\chi_s(q) = \frac{\chi^0(q)}{1 - U\chi^0(q)}, \quad \chi_c(q) = \frac{\chi^0(q)}{1 + U\chi^0(q)}, \quad (7)$$

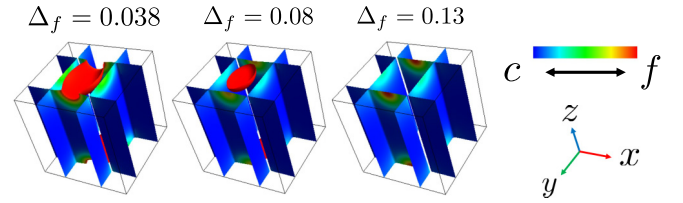


FIG. 1. Fermi surfaces of the mixed-dimensional PAM. The  $f$ -electron level  $\Delta_f$  is varied from 0.038 to 0.13. The weight of  $f$  electrons is illustrated in red, while the conduction electrons are in blue.

with the bare susceptibility

$$\chi^0(q) = -\frac{T}{N} \sum_k G_f(k+q)G_f(k). \quad (8)$$

Here,  $G_f(k)$  is the  $f$ -electron's Green's function,  $q = (\mathbf{q}, i\Omega_m)$ , and  $\Omega_m = 2m\pi T$  are bosonic Matsubara frequencies. We investigate superconductivity in this model by solving the Eliashberg equation [17] with the effective interactions given by the RPA,

$$V^s(k-k') = U + \frac{3}{2}U^2\chi_s(k-k') - \frac{1}{2}U^2\chi_c(k-k'), \quad (9)$$

$$V^t(k-k') = -\frac{1}{2}U^2\chi_s(k-k') - \frac{1}{2}U^2\chi_c(k-k'), \quad (10)$$

where the subscript  $s$  and  $t$  represent the spin-singlet and spin-triplet Cooper pairing channels, respectively. The instability of superconductivity is examined by the linearized Eliashberg equation

$$\lambda \Delta(k) = -\frac{T}{N} \sum_{k'} V(k-k') |G_f(k')|^2 \Delta(k'). \quad (11)$$

The superconducting transition temperature is determined by the condition  $\lambda = 1$ . In the following, we discuss superconducting states by calculating the eigenvalue  $\lambda$ . The larger  $\lambda$  indicates a higher transition temperature. The numerical calculations are carried out for the  $N = 64 \times 64 \times 64$  lattice and the Matsubara frequency cutoff  $N_f = 1024$ .

## III. FERMI SURFACE

First, we show the Fermi surfaces of the model. Later we see that magnetic fluctuations drastically change depending on the shape of the Fermi surfaces, which is mainly determined by  $\Delta_f$  and  $V_{fp}$ . As shown in Fig. 1, when we decrease the  $f$ -electron level  $\Delta_f$ , the Lifshitz transitions successively occur. When we set  $\Delta_f = 0.13$ , two-dimensional rectangular-shaped Fermi surfaces appear as a consequence of the hybridization of one-dimensional  $p$ - and  $d$ -electron bands. A considerable weight of  $f$  electrons also exists on the two-dimensional Fermi surfaces owing to the  $c$ - $f$  hybridization. A small three-dimensional Fermi surface is present when we decrease the  $f$ -electron level as  $\Delta_f = 0.08$ . By further decreasing  $\Delta_f$ , the three-dimensional Fermi surface is expanded and connected with the two-dimensional Fermi surfaces (see Fig. 1 for  $\Delta_f = 0.038$ ). A similar change in Fermi surfaces was reported in the band-structure calculations for  $\text{UTe}_2$ . The DFT+ $U$  and DFT+DMFT calculations for a large Coulomb interaction concluded two-dimensional Fermi

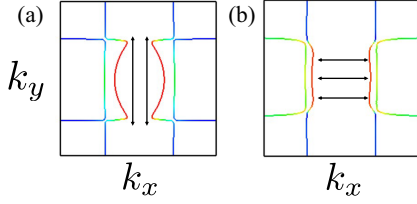


FIG. 2. Fermi surfaces on the  $k_z = \pi$  plane for  $\Delta_f = 0.05$ . (a)  $V_{fp} = 0.05$  and (b)  $V_{fp} = 0.26$ . The weight of  $f$  electrons is shown by color as in Fig. 1, and nesting vectors are illustrated by arrows.

surfaces similar to our model for  $\Delta_f = 0.13$  [8,26,27], while the DFT+ $U$  calculation for an intermediate Coulomb interaction obtained mixed-dimensional Fermi surfaces as reproduced in our model for  $\Delta_f = 0.038$  [8]. Thus, the parameter  $\Delta_f$  in our model may correspond to the interaction parameter of  $\text{UTe}_2$ .

In heavy-fermion systems, quantum phase transitions are often tunable by applied pressure, which has been interpreted as an increase in hybridization between  $f$  electrons and conduction electrons. The following results in our model are also sensitive to the hybridization parameter  $V_{fp}$ , which affects the shape of the three-dimensional Fermi surface rather than its size. We show the Fermi surfaces for various  $V_{fp}$  in Fig. 2. Interestingly, the nesting property changes with  $V_{fp}$ , as illustrated in the figure. Since the nesting vector is essential for the peak position of the magnetic fluctuations and resulting superconducting property, the magnetic fluctuations and the superconducting state change as varying the hybridization parameter  $V_{fp}$  which will be discussed as an effect of applied pressure. However, we have confirmed that magnetic fluctuations are not sensitive to another hybridization parameter  $V_{fd}$  and then fixed  $V_{fd}$  for the following discussion.

#### IV. SPIN SUSCEPTIBILITY

Second, we discuss magnetic fluctuations. Our mixed-dimensional PAM shows ferromagnetic fluctuation, antiferromagnetic fluctuation, and their coexistence depending on the parameters discussed above. Antiferromagnetic fluctuation is dominant for the  $f$ -electron level  $\Delta_f$  ranging from 0.038 to 0.054, while ferromagnetic fluctuation is dominant for  $\Delta_f$  from 0.055 to 0.13. To focus on the parameter dependence, we set the Coulomb interaction so that the Stoner factor is  $\max U\chi^0(q) = 0.98$ . Magnetic susceptibility on the  $q_z = 0$  plane is shown in Fig. 3.

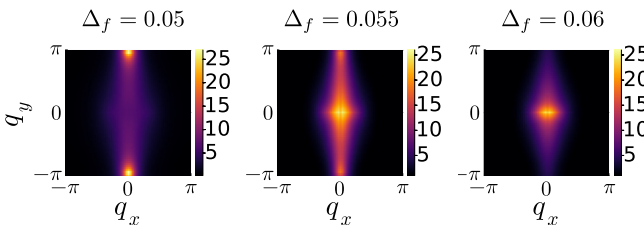


FIG. 3. Static spin susceptibility  $\chi_s(\mathbf{q}) \equiv \chi_s(\mathbf{q}, i\Omega_m = 0)$  on the  $q_z = 0$  plane for various  $f$ -electron levels  $\Delta_f$ .

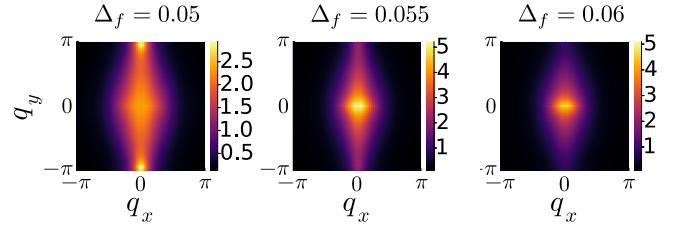


FIG. 4. Spin susceptibility integrated along the  $q_z$  direction, defined by  $\chi_z^{2D}(q_x, q_y) \equiv \int \chi_s(\mathbf{q}) dq_z$ .

In the result for  $\Delta_f = 0.05$ , we see an antiferromagnetic fluctuation with the wave vector around  $\mathbf{q} = (0, \pi, 0)$ , consistent with the neutron scattering experiments [11,12]. Thus, the antiferromagnetic fluctuation in  $\text{UTe}_2$  can be explained by the nesting vector of Fermi surfaces with substantial  $f$  electrons, as shown in Fig. 2(a). On the other hand, when we slightly increase the  $f$ -electron level as  $\Delta_f = 0.055$ , a ferromagnetic fluctuation with the wave vector  $\mathbf{q} = \mathbf{0}$  becomes dominant and coexists with the antiferromagnetic fluctuation. Ferromagnetic fluctuation naturally arises from the three-dimensional property of  $f$  electrons. Thus, (anti)ferromagnetic fluctuations are sensitive to the parameters, and they can coexist. This finding may be consistent with the fact that a ferromagnetic correlation has been suggested in  $\text{UTe}_2$  [6,7,9,10,57] and coexisting ferro- and antiferromagnetic fluctuations were reported [27,58].

In our model, the magnetic susceptibility always shows a maximum on the  $q_z = 0$  plane. To get information on magnetic fluctuations away from  $q_z = 0$ , Fig. 4 shows the integration of spin susceptibility for  $q_z$ . Even for  $\Delta_f = 0.05$  resulting in a dominant antiferromagnetic fluctuation, the magnetic fluctuation has substantial weight around  $(q_x, q_y) = (0, 0)$ , indicating a two-dimensional ferromagnetic correlation. Because a two-dimensional fluctuation generally favors superconductivity [17], the ferromagnetic correlation is expected to be important for superconductivity.

As shown above, the mixed-dimensional PAM reproduces both ferromagnetic and antiferromagnetic fluctuations that have been considered to exist in  $\text{UTe}_2$ . The three-dimensional  $f$  electrons are crucially important for the magnetic fluctuations [56]. Furthermore, the model is consistent with a previous study of the 24-band PAM [37], in which an antiferromagnetic fluctuation with the wave vector  $\mathbf{q} \simeq (\pi, 0, 0)$  develops by increasing  $c$ - $f$  hybridization. Figure 5 shows the spin susceptibility in the mixed-dimensional PAM for strong hybridization. We see that the wave vector of

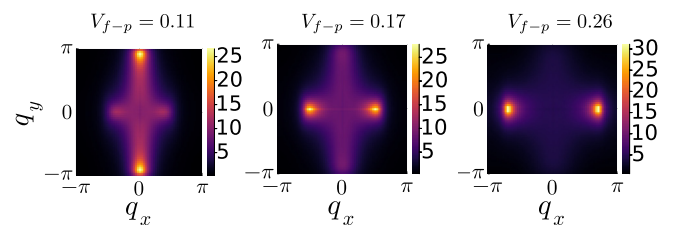


FIG. 5. Spin susceptibility on the  $q_z = 0$  plane for various hybridization parameters  $V_{fp}$ . We fix the  $f$ -electron level  $\Delta_f = 0.05$ .

TABLE I. Irreducible representations and basis functions of the  $D_{2h}$  point group.

IR ( $D_{2h}$ )	$A_g$	$B_{1g}$	$B_{2g}$	$B_{3g}$	$A_u$	$B_{1u}$	$B_{2u}$	$B_{3u}$
Basis function	1	$k_x k_y$	$k_x k_z$	$k_y k_z$	$k_x k_y k_z$	$k_z$	$k_y$	$k_x$

antiferromagnetic fluctuation gradually changes from  $\mathbf{q} \simeq (0, \pi, 0)$  to  $\mathbf{q} \simeq (\pi, 0, 0)$ . This is because strong hybridization changes the Fermi surfaces and results in better nesting along the  $x$  direction as shown in Fig. 2(b).

## V. SUPERCONDUCTIVITY

Next, we study superconductivity mediated by magnetic fluctuations. In particular, we focus on the relation between the wave vector of magnetic fluctuations and the symmetry of superconductivity.

For this purpose, we solve the linearized Eliashberg equation for all the irreducible representations of the  $D_{2h}$  point group. Note that the model in this study does not include a spin-orbit coupling. Therefore, we classify the gap function  $\Delta(k)$  by the representation without a spin degree of freedom. Table I shows the list of irreducible representations and basis functions. In this classification, the  $B_{1u}$ ,  $B_{2u}$ , and  $B_{3u}$  representations correspond to the  $p$ -wave superconductivity while the  $A_u$  representation corresponds to the  $f$ -wave superconductivity. The other representations indicate spin-singlet superconductivity with either  $s$ -wave or  $d$ -wave symmetry.

First, we show Fig. 6 for the  $\Delta_f$  dependence of eigenvalues of the Eliashberg equation. We see that the spin-triplet  $p$ -wave superconductivity of  $B_{1u}$  and  $B_{3u}$  representations is stable over a wide range of parameters. In particular, the  $p$ -wave superconductivity is stable even around  $\Delta_f = 0.05$  where antiferromagnetic fluctuation is dominant. This is because the ferromagnetic fluctuation and antiferromagnetic fluctuation cooperatively stabilize the  $p$ -wave superconductivity. Indeed, the  $p$ -wave superconductivity is most stable when the two

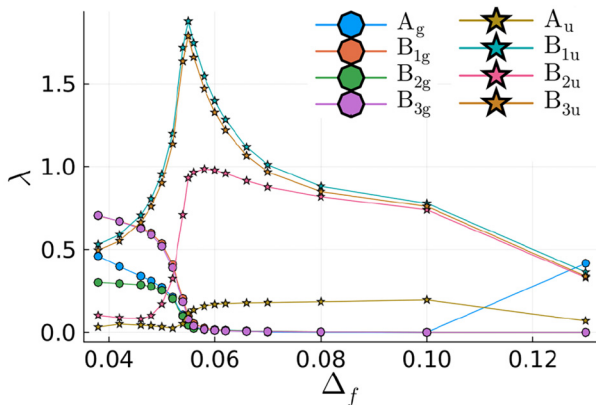


FIG. 6. Eigenvalues of the Eliashberg equation as functions of the  $f$ -electron level  $\Delta_f$ . The maximum values for each irreducible representation are shown. Spin-triplet superconductivity and spin-singlet superconductivity are plotted by stars and circles, respectively.

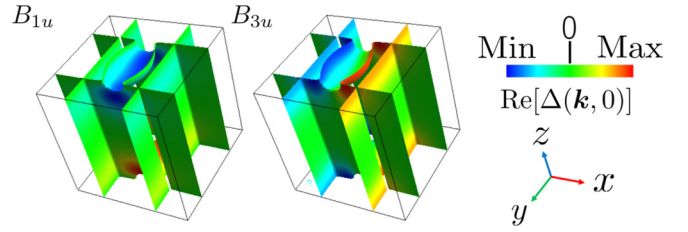


FIG. 7. Gap functions of  $B_{1u}$  and  $B_{3u}$  representations on the Fermi surfaces. The color represents the real part of the gap functions.

fluctuations coexist, as the eigenvalue  $\lambda$  shows the maximum around  $\Delta_f = 0.055$ .

The antiferromagnetic fluctuation can favor spin-triplet superconductivity when the gap function has the same sign between the Fermi momentum connected by the nesting vector [15–17]. This condition is indeed satisfied for the  $B_{1u}$  and  $B_{3u}$  representations. Figure 7 shows the gap functions on the Fermi surfaces for  $\Delta_f = 0.05$ , where the static gap function is defined as

$$\Delta(\mathbf{k}, 0) \equiv \frac{\Delta(\mathbf{k}, i\pi T) + \Delta(\mathbf{k}, -i\pi T)}{2}. \quad (12)$$

The antiferromagnetic fluctuation with  $\mathbf{q} = (0, \pi, 0)$  acts as an attractive force for the  $B_{1u}$  and  $B_{3u}$  representations because the gap functions on the Fermi surface do not change the sign for magnetic scattering. However, it gives a repulsive interaction for the  $B_{2u}$  representation, and thus the  $B_{2u}$  state is suppressed. For  $\Delta_f > 0.08$ , all the  $p$ -wave superconducting states are nearly degenerate, because the antiferromagnetic fluctuation is negligible and the ferromagnetic fluctuation equally favors all the  $p$ -wave superconducting states. In the following, we fix the crystal field parameter  $\Delta_f = 0.05$ , where the ferromagnetic and antiferromagnetic fluctuations coexist and the  $B_{1u}$  and  $B_{3u}$  states are stable and nearly degenerate.

Next, we show the hybridization  $V_{fp}$  dependence of superconductivity. In Fig. 8, we see that stable superconducting states are the spin-triplet  $B_{1u}$  and  $B_{3u}$  states for small  $V_{fp}$ , while the spin-singlet  $B_{1g}$  and  $B_{2g}$  states are stable for large  $V_{fp}$ . This can be regarded as a parity transition of superconductivity, where the symmetry of superconductivity changes

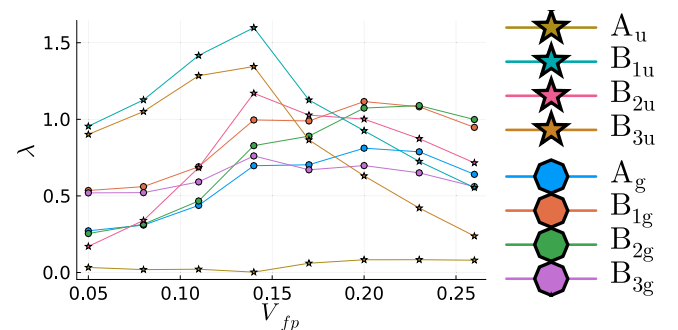


FIG. 8. The hybridization dependence of superconductivity, indicated by the eigenvalues  $\lambda$  of the Eliashberg equation. We set  $\Delta_f = 0.05$ .

from odd parity to even parity by increasing the magnitude of hybridization. Accompanied by the development of antiferromagnetic fluctuations with a  $\mathbf{q} \parallel \hat{x}$  component, the spin-singlet superconductivity is favored. Similar results have been obtained in the 24-band PAM [37] and the model of two-dimensional Fermi surfaces [16], where spin-singlet superconductivity is stable due to the magnetic fluctuations with a large  $\mathbf{q} \parallel \hat{x}$  component. Phenomenological models assuming magnetic wave vectors were also studied in Ref. [16] and comparable spin-triplet superconductivity is obtained in some cases. The hybridization dependence obtained above is qualitatively consistent with the 24-band PAM [37], where the extended  $s$ -wave state is stable instead of the  $d$ -wave one. Since the hybridization is expected to be enhanced by pressure in heavy-fermion systems, the parity transition may correspond to the multiple superconducting phases of  $\text{UTe}_2$  [7,44]. However, the pressure and magnetic fields also change the electronic state through the  $f$ -electron level  $\Delta_f$ , the Coulomb interaction  $U$ , and others. Therefore, further study based on first-principles calculations combined with experiments is desirable.

The difference between the superconducting states in regions of small and large  $V_{fp}$ , which is caused by changes in the momentum dependence of magnetic fluctuations, can be interpreted based on the real-space picture. Antiferromagnetic fluctuations with  $\mathbf{q} \parallel \hat{y}$  are compatible with the ferromagnetic correlation along the one-dimensional U ladders aligned with the  $a$  axis, as suggested by the neutron scattering experiment [12], while those with  $\mathbf{q} \parallel \hat{x}$  indicate an antiferromagnetic correlation in the ladder. The former can stabilize spin-triplet superconductivity while the latter stabilizes spin-singlet superconductivity. Therefore, our results imply that the (anti)ferromagnetic correlation in the U ladder is essential for superconductivity in  $\text{UTe}_2$ .

## VI. SUMMARY AND DISCUSSION

In this paper, we have proposed the  $(1+3)$ -dimensional PAM as a minimal model for Fermi surfaces, magnetic fluctuations, and superconductivity in  $\text{UTe}_2$ . The model reproduces the antiferromagnetic and ferromagnetic fluctuations which have been indicated by experiments. The spin-triplet superconductivity is cooperatively stabilized by these magnetic fluctuations. We emphasize that the spin-triplet  $p$ -wave superconductivity is stable against spin-singlet superconductivity near the antiferromagnetic quantum critical point in contrast

to many other microscopic models. This is a characteristic property of the  $(1+3)$ -dimensional model, as we find that spin-triplet superconductivity and antiferromagnetic fluctuation are exclusive in the  $(1+2)$ -dimensional PAM [56].

We can extend the mixed-dimensional PAM to include spin-orbit coupling, magnetic fields, and multiple orbitals and sublattices. Thus, we expect that the model will be the basis of further theoretical studies for  $\text{UTe}_2$ . While our calculation indicates the  $k_x$  and  $k_z$  orbital components of order parameters, the spin-triplet superconducting states are degenerate because of the spin component. Spin-orbit coupling and magnetic fields break the spin  $\text{SU}(2)$  symmetry and play essential roles in determining the spin component. Thus, calculations containing these effects are desirable in the future to identify the multiple superconducting phases under pressures [7,44–51] and/or magnetic fields [7,52–55,59]. Recently, development in the high-purity crystal growth [29] makes a second era in experiments of  $\text{UTe}_2$ . For instance, the quantum oscillation was detected [30–33], and the thermal conductivity [34] and NMR Knight shift [60] show behaviors consistent with the order parameter  $\mathbf{d} = k_x\hat{x} + k_y\hat{y} + k_z\hat{z}$ , similar to the B phase of  $^3\text{He}$  [61]. The order parameter contains the  $k_x$  and  $k_z$  orbital components consistent with our results and realizes strong (weak) topological superconductivity in the presence (absence) of a three-dimensional Fermi surface [8,62]. Since other pairing states have also been suggested experimentally [63,64], further studies are needed to elucidate the symmetry of superconductivity in  $\text{UTe}_2$ .

*Note added.* Recently, we became aware of a work in which the magnetic wave vector of the antiferromagnetic phase at high pressure has been reported experimentally [65]. The result is  $(q_x, q_y) = (0.07, 0.33) \times 2\pi$ , which is qualitatively consistent with our prediction in that  $q_x$  increases and  $q_y$  decreases under pressure, but the change is rather small. The impact of this magnetic fluctuation on superconductivity should be studied in a separate work.

## ACKNOWLEDGMENTS

We appreciate helpful discussions with J. Ishizuka, D. Aoki, J.-P. Brison, K. Ishida, G. Knebel, Y. Matsuda, H. Sakai, S. Suetsugu, Y. Tokiwa, and Y. Tokunaga. We use FermiSurfer to describe the Fermi surfaces in this paper [66]. This work was supported by JSPS KAKENHI (Grants No. 21K18145, No. 22H01181, No. 22H04933, and No. 22KJ1716).

- 
- [1] A. P. Schnyder, S. Ryu, A. Furusaki, and A. W. W. Ludwig, *Phys. Rev. B* **78**, 195125 (2008).
  - [2] M. Sato, *Phys. Rev. B* **81**, 220504(R) (2010).
  - [3] L. Fu and E. Berg, *Phys. Rev. Lett.* **105**, 097001 (2010).
  - [4] M. Sato and S. Fujimoto, *J. Phys. Soc. Jpn.* **85**, 072001 (2016).
  - [5] J. Linder and J. W. A. Robinson, *Nat. Phys.* **11**, 307 (2015).
  - [6] S. Ran, C. Eckberg, Q. P. Ding, Y. Furukawa, T. Metz, S. R. Saha, I. L. Liu, M. Zic, H. Kim, J. Paglione, and N. P. Butch, *Science* **365**, 684 (2019).
  - [7] D. Aoki, J.-P. Brison, J. Flouquet, K. Ishida, G. Knebel, Y. Tokunaga, and Y. Yanase, *J. Phys.: Condens. Matter* **34**, 243002 (2022).
  - [8] J. Ishizuka, S. Sumita, A. Daido, and Y. Yanase, *Phys. Rev. Lett.* **123**, 217001 (2019).
  - [9] S. Sundar, S. Gheidi, K. Akintola, A. M. Côté, S. R. Dunsiger, S. Ran, N. P. Butch, S. R. Saha, J. Paglione, and J. E. Sonier, *Phys. Rev. B* **100**, 140502(R) (2019).
  - [10] Y. Tokunaga, H. Sakai, S. Kambe, T. Hattori, N. Higa, G. Nakamine, S. Kitagawa, K. Ishida, A. Nakamura, Y. Shimizu, Y. Homma, D. X. Li, F. Honda, and D. Aoki, *J. Phys. Soc. Jpn.* **88**, 073701 (2019).
  - [11] C. Duan, K. Sasmal, M. B. Maple, A. Podlesnyak, J.-X. Zhu, Q. Si, and P. Dai, *Phys. Rev. Lett.* **125**, 237003 (2020).

- [12] W. Knafo, G. Knebel, P. Steffens, K. Kaneko, A. Rosuel, J.-P. Brison, J. Flouquet, D. Aoki, G. Lapertot, and S. Raymond, *Phys. Rev. B* **104**, L100409 (2021).
- [13] C. Duan, R. E. Baumbach, A. Podlesnyak, Y. Deng, C. Moir, A. J. Breindel, M. B. Maple, E. M. Nica, Q. Si, and P. Dai, *Nature (London)* **600**, 636 (2021).
- [14] S. Raymond, W. Knafo, G. Knebel, K. Kaneko, J.-P. Brison, J. Flouquet, D. Aoki, and G. Lapertot, *J. Phys. Soc. Jpn.* **90**, 113706 (2021).
- [15] K. Kuroki, R. Arita, and H. Aoki, *Phys. Rev. B* **63**, 094509 (2001).
- [16] A. Kreisler, Y. Quan, and P. J. Hirschfeld, *Phys. Rev. B* **105**, 104507 (2022).
- [17] Y. Yanase, T. Jujo, T. Nomura, H. Ikeda, T. Hotta, and K. Yamada, *Phys. Rep.* **387**, 1 (2003).
- [18] K. Kuroki, *J. Phys. Soc. Jpn.* **75**, 051013 (2006).
- [19] T. Kuwabara and M. Ogata, *Phys. Rev. Lett.* **85**, 4586 (2000).
- [20] M. Sato and M. Kohmoto, *J. Phys. Soc. Jpn.* **69**, 3505 (2000).
- [21] K. Kuroki, M. Ogata, R. Arita, and H. Aoki, *Phys. Rev. B* **63**, 060506(R) (2001).
- [22] J. Tei, T. Mizushima, and S. Fujimoto, *Phys. Rev. B* **109**, 064516 (2024).
- [23] Y. Yanase and M. Ogata, *J. Phys. Soc. Jpn.* **72**, 673 (2003).
- [24] Y. Tanaka and K. Kuroki, *Phys. Rev. B* **70**, 060502(R) (2004).
- [25] K. Kuroki and Y. Tanaka, *J. Phys. Soc. Jpn.* **74**, 1694 (2005).
- [26] L. Miao, S. Liu, Y. Xu, E. C. Kotta, C.-J. Kang, S. Ran, J. Paglione, G. Kotliar, N. P. Butch, J. D. Denlinger, and L. A. Wray, *Phys. Rev. Lett.* **124**, 076401 (2020).
- [27] Y. Xu, Y. Sheng, and Y.-f. Yang, *Phys. Rev. Lett.* **123**, 217002 (2019).
- [28] S.-i. Fujimori, I. Kawasaki, Y. Takeda, H. Yamagami, A. Nakamura, Y. Homma, and D. Aoki, *J. Phys. Soc. Jpn.* **90**, 015002 (2021).
- [29] H. Sakai, P. Opletal, Y. Tokiwa, E. Yamamoto, Y. Tokunaga, S. Kambe, and Y. Haga, *Phys. Rev. Mater.* **6**, 073401 (2022).
- [30] D. Aoki, H. Sakai, P. Opletal, Y. Tokiwa, J. Ishizuka, Y. Yanase, H. Harima, A. Nakamura, D. Li, Y. Homma, Y. Shimizu, G. Knebel, J. Flouquet, and Y. Haga, *J. Phys. Soc. Jpn.* **91**, 083704 (2022).
- [31] D. Aoki, I. Sheikin, A. McCollam, J. Ishizuka, Y. Yanase, G. Lapertot, J. Flouquet, and G. Knebel, *J. Phys. Soc. Jpn.* **92**, 065002 (2023).
- [32] A. G. Eaton, T. I. Weinberger, N. J. M. Popiel, Z. Wu, A. J. Hickey, A. Cabala, J. Pospisil, J. Prokleska, T. Haidamak, G. Bastien, P. Opletal, H. Sakai, Y. Haga, R. Nowell, S. M. Benjamin, V. Sechovsky, G. G. Lonzarich, F. M. Grosche, and M. Valiska, *Nat. Commun.* **15**, 223 (2024).
- [33] C. Broyles, Z. Rehfuss, H. Siddiquee, J. A. Zhu, K. Zheng, M. Nikolo, D. Graf, J. Singleton, and S. Ran, *Phys. Rev. Lett.* **131**, 036501 (2023).
- [34] S. Suetsugu, M. Shimomura, M. Kamimura, T. Asaba, H. Asaeda, Y. Kosuge, Y. Sekino, S. Ikemori, Y. Kasahara, Y. Kohsaka, M. Lee, Y. Yanase, H. Sakai, P. Opletal, Y. Tokiwa, Y. Haga, and Y. Matsuda, *Sci. Adv.* **10**, adk3372 (2024).
- [35] Y. S. Eo, S. Liu, S. R. Saha, H. Kim, S. Ran, J. A. Horn, H. Hodovanets, J. Colliner, T. Metz, W. T. Fuhrman, A. H. Nevidomskyy, J. D. Denlinger, N. P. Butch, M. S. Fuhrer, L. A. Wray, and J. Paglione, *Phys. Rev. B* **106**, L060505 (2022).
- [36] T. Shishidou, H. G. Suh, P. M. R. Brydon, M. Weinert, and D. F. Agterberg, *Phys. Rev. B* **103**, 104504 (2021).
- [37] J. Ishizuka and Y. Yanase, *Phys. Rev. B* **103**, 094504 (2021).
- [38] T. Hazra and P. Coleman, *Phys. Rev. Lett.* **130**, 136002 (2023).
- [39] L. Chen, H. Hu, C. Lane, E. M. Nica, J.-X. Zhu, and Q. Si, [arXiv:2112.14750](https://arxiv.org/abs/2112.14750).
- [40] D. Shaffer and D. V. Chichinadze, *Phys. Rev. B* **106**, 014502 (2022).
- [41] H. C. Choi, S. H. Lee, and B.-J. Yang, [arXiv:2206.04876](https://arxiv.org/abs/2206.04876).
- [42] J. J. Yu, Y. Yu, D. F. Agterberg, and S. Raghu, *Phys. Rev. B* **107**, 214510 (2023).
- [43] D. Aoki, K. Ishida, and J. Flouquet, *J. Phys. Soc. Jpn.* **88**, 022001 (2019).
- [44] D. Braithwaite, M. Vališka, G. Knebel, G. Lapertot, J. P. Brison, A. Pourret, M. E. Zhitomirsky, J. Flouquet, F. Honda, and D. Aoki, *Commun. Phys.* **2**, 147 (2019).
- [45] D. Aoki, F. Honda, G. Knebel, D. Braithwaite, A. Nakamura, D. Li, Y. Homma, Y. Shimizu, Y. J. Sato, J.-P. Brison, and J. Flouquet, *J. Phys. Soc. Jpn.* **89**, 053705 (2020).
- [46] W. C. Lin, D. J. Campbell, S. Ran, I. L. Liu, H. Kim, A. H. Nevidomskyy, D. Graf, N. P. Butch, and J. Paglione, *npj Quantum Mater.* **5**, 68 (2020).
- [47] S. Ran, H. Kim, I. L. Liu, S. R. Saha, I. Hayes, T. Metz, Y. S. Eo, J. Paglione, and N. P. Butch, *Phys. Rev. B* **101**, 140503(R) (2020).
- [48] S. M. Thomas, F. B. Santos, M. H. Christensen, T. Asaba, F. Ronning, J. D. Thompson, E. D. Bauer, R. M. Fernandes, G. Fabbris, and P. F. Rosa, *Sci. Adv.* **6**, eabc8709 (2020).
- [49] G. Knebel, M. Kimata, M. Vališka, F. Honda, D. Li, D. Braithwaite, G. Lapertot, W. Knafo, A. Pourret, Y. J. Sato, Y. Shimizu, T. Kihara, J.-P. Brison, J. Flouquet, and D. Aoki, *J. Phys. Soc. Jpn.* **89**, 053707 (2020).
- [50] D. Aoki, M. Kimata, Y. J. Sato, G. Knebel, F. Honda, A. Nakamura, D. Li, Y. Homma, Y. Shimizu, W. Knafo, D. Braithwaite, M. Vališka, A. Pourret, J.-P. Brison, and J. Flouquet, *J. Phys. Soc. Jpn.* **90**, 074705 (2021).
- [51] P. F. S. Rosa, A. Weiland, S. S. Fender, B. L. Scott, F. Ronning, J. D. Thompson, E. D. Bauer, and S. M. Thomas, *Commun. Mater.* **3**, 33 (2022).
- [52] A. Rosuel, C. Marcenat, G. Knebel, T. Klein, A. Pourret, N. Marquardt, Q. Niu, S. Rousseau, A. Demuer, G. Seyfarth, G. Lapertot, D. Aoki, D. Braithwaite, J. Flouquet, and J. P. Brison, *Phys. Rev. X* **13**, 011022 (2023).
- [53] H. Sakai, Y. Tokiwa, P. Opletal, M. Kimata, S. Awaji, T. Sasaki, D. Aoki, S. Kambe, Y. Tokunaga, and Y. Haga, *Phys. Rev. Lett.* **130**, 196002 (2023).
- [54] Y. Tokiwa, P. Opletal, H. Sakai, K. Kubo, E. Yamamoto, S. Kambe, M. Kimata, S. Awaji, T. Sasaki, D. Aoki, Y. Tokunaga, and Y. Haga, [arXiv:2210.11769](https://arxiv.org/abs/2210.11769).
- [55] S. Ran, I.-L. Liu, Y. S. Eo, D. J. Campbell, P. M. Neves, W. T. Fuhrman, S. R. Saha, C. Eckberg, H. Kim, D. Graf, F. Balakirev, J. Singleton, J. Paglione, and N. P. Butch, *Nat. Phys.* **15**, 1250 (2019).
- [56] See Supplemental Material at <http://link.aps.org/supplemental/10.1103/PhysRevB.109.104509> for the results of the  $(1+2)$ -dimensional periodic Anderson model.
- [57] H. Fujibayashi, K. Kinjo, G. Nakamine, S. Kitagawa, K. Ishida, Y. Tokunaga, H. Sakai, S. Kambe, A. Nakamura, Y. Shimizu, Y. Homma, D. Li, F. Honda, and D. Aoki, *J. Phys. Soc. Jpn.* **92**, 053702 (2023).

- [58] D. V. Ambika, Q.-P. Ding, K. Rana, C. E. Frank, E. L. Green, S. Ran, N. P. Butch, and Y. Furukawa, *Phys. Rev. B* **105**, L220403 (2022).
- [59] K. Kinjo, H. Fujibayashi, S. Kitagawa, K. Ishida, Y. Tokunaga, H. Sakai, S. Kambe, A. Nakamura, Y. Shimizu, Y. Homma, D. X. Li, F. Honda, D. Aoki, K. Hiraki, M. Kimata, and T. Sasaki, *Phys. Rev. B* **107**, L060502 (2023).
- [60] H. Matsumura, H. Fujibayashi, K. Kinjo, S. Kitagawa, K. Ishida, Y. Tokunaga, H. Sakai, S. Kambe, A. Nakamura, Y. Shimizu, Y. Homma, D. Li, F. Honda, and D. Aoki, *J. Phys. Soc. Jpn.* **92**, 063701 (2023).
- [61] A. J. Leggett, *Rev. Mod. Phys.* **47**, 331 (1975).
- [62] J. Tei, T. Mizushima, and S. Fujimoto, *Phys. Rev. B* **107**, 144517 (2023).
- [63] K. Ishihara, M. Roppongi, M. Kobayashi, K. Imamura, Y. Mizukami, H. Sakai, P. Opletal, Y. Tokiwa, Y. Haga, K. Hashimoto, and T. Shibauchi, *Nat. Commun.* **14**, 2966 (2023).
- [64] Z. Li, C. M. Moir, N. J. McKee, E. Lee-Wong, R. E. Baumbach, M. B. Maple, and Y. Liu, [arXiv:2309.08668](https://arxiv.org/abs/2309.08668).
- [65] W. Knafo, T. Thebault, P. Manuel, D. D. Khalyavin, F. Orlandi, E. Ressouche, K. Beauvois, G. Lapertot, K. Kaneko, D. Aoki, D. Braithwaite, G. Knebel, and S. Raymond, [arXiv:2311.05455](https://arxiv.org/abs/2311.05455).
- [66] M. Kawamura, *Comput. Phys. Commun.* **239**, 197 (2019).